ACS Combinatorial Science

Research Article

pubs.acs.org/acscombsci

Spatially Resolved Solid-State ^{1}H NMR for Evaluation of Gradient-Composition Polymeric Libraries

Johannes Leisen,*[†] Ismael J. Gomez,[‡] John A. Roper, III,[∥] J. Carson Meredith,[‡] and Haskell W. Beckham[§]

[†]School of Chemistry and Biochemistry, [‡]School of Chemical and Biomolecular Engineering, and [§]School of Materials Science and Engineering, Georgia Institute of Technology, Atlanta, Georgia 30332, United States

[∥]The Dow Chemical Company, Midland, Michigan 48674, United States

ABSTRACT: Polyurethane libraries consisting of films with composition gradients of aliphatic polyisocyanate and hydroxy-terminated polyacrylate resin were characterized using methods of ^{1}H NMR microimaging (i.e., magnetic resonance imaging, (MRI)) and solid-state NMR. Molecular mobilities and underlying structural information were extracted as a function of the relative content of each of the two components. Routine NMR microimaging using the spin-echo sequence only allows investigations of transverse relaxation of magnetization at echo times >2 ms. A single-exponential decay was found, which is likely due to free, noncross-linked polymer chains. The mobility of these chains decreases with increasing content of the aliphatic polyisocyanate. The concept of a 1D NMR profiler is introduced as a novel modality for library screening, which allows the convenient measurement of static solid-state NMR spectra as a function of spatial location along a library sample that is repositioned in the rf coil between experiments. With this setup the complete transverse relaxation function was measured using Bloch decays and spin echoes. For all positions within the gradient-composition film, relaxation data consisted of at least three components that were attributed to a rigid highly cross-linked resin, an intermediate cross-linked but mobile constituent, and the highly mobile free polymer chains (the latter is also detectable by MRI). Analysis of this overall relaxation function measured via Bloch decays and spin echoes revealed only minor changes in the mobilities of the individual fractions. Findings with respect to the most mobile components are consistent with the results obtained by NMR microimaging. The major effect is the significant increase in the rigid-component fraction with the addition of the hydroxy-terminated polyacrylate resin.

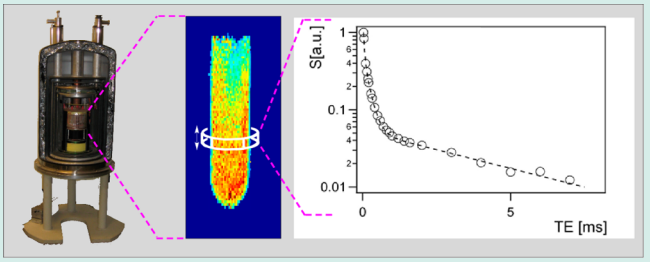

KEYWORDS: *polymer formulation, gradient composition libraries, nuclear magnetic resonance, magnetic resonance imaging, IR microscopy*

1. INTRODUCTION

Polymeric materials as used in most commodity and specialty products are based on multicomponent formulations. Often these formulations consist of a complex copolymer and a variety of additives such as stabilizers, plasticizers, and the like.[1] Hence, the development of polymer formulations can be a very labor-intensive task and there is an interest to facilitate this via high-throughput or combinatorial methods. A specific challenge for these methods in the field of polymeric materials is based on the fact that formulations for polymers are developed with the aim of specific macroscopic end-use properties such as mechanical stiffness and scratch resistance. A combinatorial library/high-throughput screening method must therefore be able to systematically characterize a polymer formulation with respect to measurable end-use properties. Numerous approaches have been described in recent reviews.[2−9] For example, polymer libraries (i.e., formulations) are fabricated with either gradient or discrete variations in composition along a given sample axis.[10−14] High-throughput mechanical characterization at individual positions within gradient-composition films has been performed using specially developed micro-mechanical testing instruments. However, given the large number of possible formulations, and the complex dependence on component interactions, additional knowledge of the physicochemical properties of polymer library films is useful to make meaningful use of the combinatorial approach. When properties affecting the mechanical response of the polymer are not already known or readily predictable, it is desirable to measure them nondestructively directly on the same polymer library. To name just one example: it is known that the mechanical properties of elastomers are affected by their chemical cross-link density.[15] To optimize the mechanical properties of an elastomer synthesized via step-growth polymerization one might systematically vary the content of a multifunctional co-monomer that leads to chemical cross-links. Consequently, it is not only important to measure the mechanical end-use properties but also the cross-link density as a function of the formulation variables. Altogether, there is a

Received: December 17, 2011
Revised: May 29, 2012
Published: June 8, 2012

need to characterize gradient-based combinatorial libraries not only with respect to the relationship between composition and end-use properties but also with respect to related physicochemical properties.

Methods of Nuclear Magnetic Resonance (NMR) have found widespread use in combinatorial science.[16,17] Most applications have focused on the characterization of chemical compounds in solution using standard NMR experiments or the characterization of gels using Magic Angle Spinning (MAS) techniques. High throughput can be achieved using sample changers or flow set-ups.[18] Less established is the use of solid-state methods[19,20] for combinatorial libraries. Such methods are ideally suited to provide a link between molecular and bulk mechanical properties in the solid state. One of the practical obstacles for the high-throughput use of solid-state NMR techniques is the automation of magic angle spinning (MAS). Even though commercial sample changers exist for MAS experiments, complete automation is not straightforward because of the elaborate procedure of packing an MAS rotor, their cost, and the often long measuring times needed for MAS experiments of nuclei other than ^{1}H or ^{19}F. These issues are irrelevant for ^{1}H solid-state NMR of static, nonspinning samples. Sample preparation can be simple and measuring times may range from a few seconds to tens of minutes, depending on the type of experiment. Most importantly, a wide variety of ^{1}H solid-state NMR experiments can be used to yield an important collection of material properties. For instance, ^{1}H solid-state NMR relaxation time measurements have been employed for high-throughput characterization of clay dispersion in polymer−clay nanocomposites.[21,22] Relaxation experiments can also yield the amount and nature of crystallites in semicrystalline polymers.[23−27] Measurements of residual ^{1}H dipolar couplings[28−31] provide information on anisotropic chain motions and therefore cross-link densities.[32−34]

To our knowledge the NMR characterization of polymeric films and libraries composed of composition gradients is completely unexplored. The obvious approach would be to extend spectroscopic or relaxometric NMR techniques with spatial resolution as it is used in Nuclear Magnetic Resonance Imaging (in clinical settings referred to as Magnetic Resonance Imaging, MRI).[35,36] The feasibility of MRI for high-throughput screening of solutions has been successfully demonstrated.[37] It has also been shown that NMR imaging may be used to assess individual NMR parameters of polymers.[35] An example includes probing the above-mentioned dipolar coupling via T_2-relaxation effects to produce spatial maps depicting the distribution of a given physical property in a sample.[38,39] Because of limited sensitivities, only a few studies have been concerned with the investigation of polymer films via NMR imaging.[40,41]

To explore the capability of MRI for the characterization of gradient-composition libraries, we have prepared polyurethane films from a polyisocyanate and a hydroxy-terminated polyacrylate in which the molar ratio of these two reactants vary along the length of the film. This film was expected to be an ideal candidate for MRI characterization using commercial microimaging equipment. The film has many commercial applications, for example, automotive coatings, and the strong dependence of cross-link density on relative component fractions was expected to lead to measurable property gradients along the film. The feasibility and challenges of MRI for the characterization of polymer gradient-composition films are discussed and demonstrated in this paper. On the basis of the MRI studies, we propose an alternative approach that we call *1D NMR profiling* that can be used for high-throughput characterization of gradient-composition samples. This simple *1D NMR profiling* approach is much more robust, and versatile as a larger variety of established NMR experiments may be employed for the characterization of gradient-composition samples. To provide a context for this development, we begin with a brief background on the basics of spatially resolved NMR.

2. BACKGROUND: SPATIALLY RESOLVED NMR

The theory of spatially resolved NMR is extensive, and we refer the reader to many excellent monographs and reviews in the field.[35,36] For the discussion of effects relevant for this study, it shall suffice to show the signal, S, detected for a single chemical site after a radio frequency pulse as a complex function of data acquisition time, t,

$$S(t) \propto \{\cos[(\omega - \omega_0)t] + i \sin[(\omega - \omega_0)t]\} \exp\left\{-\frac{t}{T_2^*}\right\} \quad (1)$$

where ω is the receiver frequency, ω_0 is the nuclear resonance frequency, and T_2^* is the time constant for magnetization decay by spin−spin relaxation. Fourier transformation of this signal, a basic Bloch decay, leads to a Lorentzian-shaped peak centered at a frequency $\omega - \omega_0$ with a width $\propto 1/T_2^*$. The peak width is a measure of the mobility of the molecules or segments of molecules giving rise to the peak. Broad peaks (short T_2^* values in the range of microseconds) are characteristic of rigid molecules/segments as found in crystallites or glasses. Narrow peaks (long T_2^* values in the range of milliseconds) are characteristic of mobile molecules/segments present in fluids or soft solids such as elastomers. This peak narrowing is caused by molecular-motion-induced averaging of quantum chemical interactions, most notably dipolar couplings and the chemical shift. For polymers, such liquid-like states exist in melts, gels, elastomers, and similarly soft micro- and nanodomains as often encountered in copolymers and blends.

The nuclear resonance frequency ω_0, and therefore the signal, depends on the strength of the applied magnetic field. Imaging is made possible by applying magnetic field gradients $\delta\mathbf{G}/\delta\mathbf{x}$ that encode nuclear positions in the measured signal. The spatial information of the object under investigation is convoluted with the spectroscopic line shapes. For materials characterized by narrow peaks/long T_2^* values, that is, soft and fluid materials, convolution of the spatial information leads to sharp images and therefore MRI works best for these materials.

A great variety of MRI techniques have been developed for measuring NMR parameters (e.g., T_2^*), which can be correlated with bulk material properties, in a spatially resolved fashion.[35,42] One of the most common methods is the spin-echo sequence, which consists of 2 rf pulses separated by a time interval $TE/2$ where TE is the echo time. This sequence leads to the build-up of a magnetization echo at time $TE/2$ after the second pulse. One major advantage of this method is the elimination of effects due to magnetic field inhomogeneities. Consequently, the relaxation constant T_2^* is replaced by T_2 according to

$$S(TE, \mathbf{x}) = SD(\mathbf{x}) \exp\left\{-\frac{TE}{T_2(\mathbf{x})}\right\} \quad (2)$$

dx.doi.org/10.1021/co200210c | ACS Comb. Sci. 2012, 14, 415−424

where SD is the spin density or concentration. Measuring images for different echo times TE_i provides a series of images in which the signal intensity at a given spatial position $\mathbf{x}$ depends on the respective spin concentration, $SD(\mathbf{x})$, and relaxation constant, $T_2(\mathbf{x})$. By fitting voxel intensities with eq 2, two images may be constructed: $SD(\mathbf{x})$ reflects the spin concentration, and $T_2(\mathbf{x})$ reflects molecular mobilities. This approach has two major practical limitations:

(i) The need to switch field gradients on and off during a spin echo sequence leads to a minimum achievable echo time (ca. 2 ms for our instrumentation). Nuclei that relax on time scales shorter than this are not detectable. Consequently, glassy or crystalline organic matter ($T_2 \leq 50\ \mu s$) cannot be studied using conventional MRI spin echo sequences.

(ii) Many polymeric materials are characterized by relaxation functions more complex than that of eq 2. It may not be possible to collect sufficient data (i.e., images) to describe such complex relaxation functions within reasonable time frames.

3. MATERIALS AND METHODS

Sample Preparation. The sample under investigation is a gradient film based on a commercial aliphatic polyisocyanate (Desmodur N-3390 from Bayer, referred to as D-N) and a hydroxy-terminated polyacrylate resin (Desmophen A-365 from Bayer, referred to as D-A). Curing a mixture of these compounds leads to a polyacrylate-based polyurethane (PU) network. The isocyanate groups in the D-N react with the hydroxyl groups in the D-A to form this cross-linked polymer network. Useful mechanical properties such as strength and toughness are developed. For our sample we chose curing conditions to prepare a gradient film that allowed us to study the effects of molar compositions using NMR.

Solutions of D-N (90 wt % in butyl acetate) and D-A (65 wt % in butyl acetate) were obtained from the manufacturer. Further dilution of D-A (57 wt % in butyl acetate) was required to match the viscosities of the two components and improve mixing. The components were fed at linearly increasing/decreasing flow rates to prepare the gradient-composition film. On the basis of the molecular weight of the individual components (M_n = 1220 g/mol for DA) and the densities of the solutions (1.13 g/mol for D-N and 0.98 g/mol for D-A) the respective volumes were calculated to prepare mixtures of the two solutions leading to the desired molar ratios of NCO:OH (0.9:0.1 to 0.1:0.9). Those volumes correspond to starting and ending volumetric flow rates of 11.43 mL/h and 0.38 mL/h for DN and 6.57 mL/h and 17.62 mL/h for DA. That is, the two solutions were infused as linear gradients between these starting and ending flow rates into a 300-μL gradient mixing chamber at a total flow rate of 18 mL/h using two computer-controlled NE-500 syringe pumps (New Era Pump Systems, Inc.). The tubular mixing chamber, constructed using a Swagelok union (SS-400-6) as the body, was equipped with an impeller (Dewalt, Inc. Model 196). The impeller shaft, sealed using Teflon tubing to prevent liquid leakage while allowing rotation, was coupled to a motor that operated at 1500 rpm. Two Teflon inlet tubes (1/8 in. outside diameter) were fitted to the base, and one Teflon outlet tube (1/8 in. outside diameter) was fitted to the chamber head. In all cases the Reynolds number in the tubing was well below the laminar flow limits ($N_{Re} \leq 2100$) for the blend, ensuring that no turbulent mixing occurred after exiting the mixer. The outlet tube connected to a horizontally mounted rectangular Teflon mold (1.25 cm width, 7.5 cm length, and 1 mm depth) with a removable Teflon cover held in place by clamps. The blend was injected into the mold and cured at 23 °C for 16 h followed by 55 °C for 1 h in a convection oven. The syringe pumps were controlled such that the gradient film extended over a length of 6 cm. IR microscopy was used to confirm the variation in chemical structure along the film length.

It is important to note that the gradient-composition films were prepared with certain specific characteristics to enable and facilitate their characterization using methods of MRI.

(i) The film was unusually thick (1 mm) to enhance the sensitivity of a two-dimensional MRI experiment. Preparing such a thick gradient-composition film of high quality with our experimental setup was quite challenging; formation of voids, caused by solvent evaporation, could not be completely avoided.

(ii) As discussed below, most standard MRI methods work only for "soft" matter; thus, the curing was performed under unusually mild conditions to produce a "rubbery" film. Further curing at higher temperatures yielded a "rigid" film that was characterized by chain dynamics that did not vary sufficiently at moderate temperatures along the composition gradient to be detected by MRI. FTIR data of our moderately cured film provided evidence that the maximum chemical conversion was not achieved, as discussed below. Furthermore, the presence of some remaining solvent with plasticizing properties cannot be excluded.

IR Microscopy. The gradient-composition PU film was characterized by attenuated total reflectance infrared (ATR-FTIR) spectroscopy. ATR-FTIR spectroscopy measurements were performed using a Bruker Vertex 80v FTIR spectrometer coupled to a Hyperion 2000 IR microscope (both Bruker-Optics) under a 20× magnification ATR objective with a Germanium crystal. The penetration depth of the ATR crystal is less than 1 μm, and the crystal area is 80−100 μm^2. The ATR-FTIR signals averaged over 64 scans were collected in the mid-IR range, 4000−400 cm^{-1} with a resolution of 4 cm^{-1}, using a KBr beamsplitter. Bruker's FTIR software was used to correct the baseline as well as the wavelength-dependent variation in penetration depth of the IR radiation for each spectrum. Principal component analyses for mean-centered data were performed using PLS toolbox (Eigenvector Research, Inc.).

NMR Imaging. The film was placed inside a test tube (outer diameter 15 mm) with the gradient-composition axis parallel to the long axis of the tube. A Bruker DSX-400 NMR spectrometer, with a magnetic field of 9.4 T corresponding to a ^1H frequency of 400 MHz, was employed with the Bruker Micro-25 NMR accessories (Bruker-Biospin). The radio-frequency (rf) coil used with this accessory had a diameter of 20 mm and an active length of about 30 mm. Since the gradient-composition film was 60-mm long, it was imaged in two separate experiments after repositioning the test tube within the rf coil. Experiments were conducted using the Bruker Paravision 3.1 software environment. A spin-echo sequence based on two rectangular rf pulses with lengths of 50 μs ($\pi/2$ pulse) and 100 μs (π-pulse) was used without slice selection. Images consisting of 128 × 128 pixels were recorded for a repetition time of TR = 2000 ms and an echo time of TE = 2.1

dx.doi.org/10.1021/co200210c | ACS Comb. Sci. 2012, 14, 415−424

ms, which is the shortest experimentally achievable echo time for our setup. Further images were recorded for *TE* values of 3.1 ms, 4.1 ms, up to 10.1 ms. This series of images was transferred to a personal computer for analysis. A home-written program in MATLAB (The MathWorks, Inc.) was used to produce parameter-selective images by fitting corresponding voxels within the series of images using eq 2.

1D NMR Profiling. Since the composition is expected to vary only along one spatial axis of the sample, we designed a simple setup that allows the full spectroscopic characterization of the film along this axis (cf. Figure 2). A representative strip

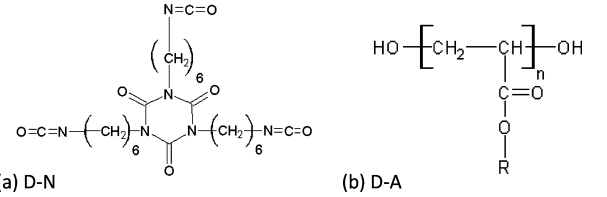

Figure 1. Components used for the preparation of the gradient-composition polyurethane film of this study: (a) D-N is Desmodur N 3390 (Bayer), a 1,6-hexamethylene diisocyanate-based polyisocyanate, and (b) D-A is Desmophen A-365 (Bayer), a hydroxy-terminated polyacrylate.

with a width of 4 mm was cut from the sample film such that the spatial axis **x** coincided with the long axis of the strip. This strip was then mounted in a glass tube with an outer diameter of 5 mm (standard NMR tube) and characterized with a Helmholtz-type rf coil with inner diameter of 5 mm and active vertical height of about 15 mm. This height was measured from images of a 5-mm NMR tube filled with water so that the water extended far beyond the top and bottom of the coil in which it was inserted. A variety of MRI pulse sequences (spin echo, gradient echo, with and without slice selection and with different pulse lengths) always provided an image that reflected fairly homogeneous excitation over the entire active range of the coil.

Adjusting the position of the test tube with respect to the rf coil allowed characterization of the gradient library at various positions along the sample strip. The spatial resolution is given by the active vertical range of the rf detection coil (ca. 15 mm for the setup reported here). Our study was conducted on a commercially available coil with through-vertical access. It is certainly possible to design a coil with smaller vertical dimensions to improve spatial resolution. While the initial experiments described in this paper were conducted by manually shifting the test tube, it should be straightforward to integrate a stepper motor into the setup to shift the sample and synchronize data acquisition to fully automate the profiler.

In many ways our 1D NMR profiler is comparable to other NMR-based explorers or profilers, some of which are commercially available,[43] that have been described in the literature to examine materials and surfaces. These instruments work mostly with low-field permanent magnets in combination with rf surface coils. The inhomogeneous magnetic and rf fields in these devices pose experimental challenges that limit the applicability of many spectroscopic pulse sequences. Our 1D NMR profiler employs conventional NMR equipment consisting of a strong and homogeneous magnetic field in combination with a homogeneous rf volume coil. Therefore, all standard solid-state NMR experiments on static samples can be conducted with this setup.

One can argue that instead of using the 1D NMR profiler, which relies on cutting a gradient strip out of a gradient-composition film, one might further cut this strip into *x*-mm-long segments, where *x* would be the spatial resolution, that can then be characterized by separate NMR experiments. While samples would have to be individually packed, automatic sample changers are commercially available. However, cutting samples into individual sections is labor intensive and obviates the need for preparing a gradient-composition film in the first place.

For the 1D NMR profiling, a Bruker AV3−400 operating at a magnetic field of 9.4 T was used. A sample strip was cut from a gradient-composition film and placed in a 5-mm (o.d.) NMR tube which was inserted into a 5-mm rf coil. This coil is part of the exchangeable set of rf coils with the Bruker Micro-25 NMR microimaging accessory. For each experiment the rf coil had to be removed from the magnet and the position of the film with respect to the sample coil was adjusted by sliding the NMR tube into the detection coil. Bloch decays were recorded within

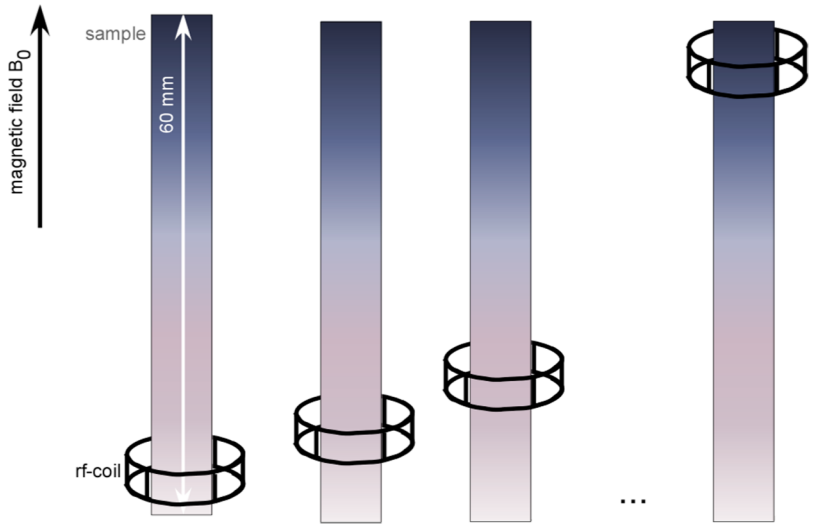

Figure 2. Schematic setup of the 1D NMR profiler. The sample is moved through the stationary rf coil in steps that depend on the sensitive field-of-view of the coil.

dx.doi.org/10.1021/co200210c | *ACS Comb. Sci.* 2012, 14, 415−424

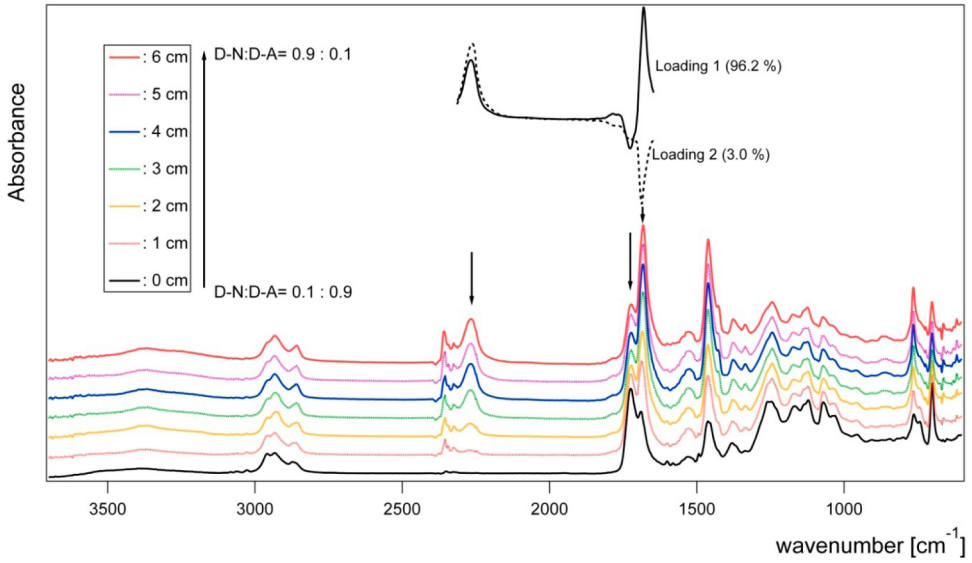

Figure 3. IR spectra recorded as a function of position (0 to 6 cm) within the gradient-composition polyurethane film. Spectra are plotted with an offset to increase visibility. Arrows point toward three prominent peaks providing information on the chemical composition and extent of conversion: 2268 cm^{-1} due to NCO stretching indicative of unreacted NCO of D-N; 1730 cm^{-1} due to C═O stretching in D-A and urethane linkages; 1680 cm^{-1} due to C═O stretching in urethane linkages and isocyanurate rings of D-N. Shown as insets are the results of a principal component analysis (loadings) investigating the spectral window containing the three peaks of interest.

Bruker's TOPSPIN software environment using a $\pi/5$ rf pulse with a length of 2 μs. Prior to every scan the rf frequency ω was adjusted to coincide exactly with the maximum of the respective NMR spectrum. A total of 1024 data points, each separated by a dwell time of DW = 4 μs was recorded. The data were transferred and analyzed with respect to their relaxation behavior according to eq 3 using Igor Pro (Wave Metric Inc.):

$$S(t) = w_{\text{rigid}} \cdot \exp(-t^2/T_2^*{}_{,\text{rigid}}) + w_{\text{inter}} \cdot \exp(-t/T_2^*{}_{,\text{inter}}) + w_{\text{mobile}} \cdot \exp(-t/T_2^*{}_{,\text{mobile}}) \quad (3)$$

in which the signal is composed of three components characterized by rigid, intermediate, and mobile chain segments. Spin-echo (SE) data were also recorded for a total of 32 values of *TE* ranging from 32.5 μs to 10 ms. The pulse lengths for the SE sequence were 5 μs ($\pi/2$ pulse) and 10 μs (π pulse).

4. RESULTS AND DISCUSSION

IR Microscopy. IR spectra were recorded as a function of spatial position within the film to obtain information on the concentration distributions of D-N, D-A, and formed cross-links (cf. Figure 3). To obtain such information, it is desirable to have at least three non-overlapping peaks in each spectrum that independently represent concentrations of each of these three species. For our experimental data, peak overlap is substantial such that no such set of 3 peaks could be identified. Furthermore, a full quantitative analysis is not possible because of missing molar extinction coefficients. Semiquantitative information on relative concentrations can be obtained via a principal component analysis (PCA).

PCA is a Chemometric tool that can provide insight into spectroscopic data that are difficult to analyze due overlap of spectral components.[44] It is based on the premise that *i* experimental spectra $\boldsymbol{Sp}_i$ may be represented by a weighted addition of a limited amount of loadings $\boldsymbol{L}_n$. For the case of mean-centered preprocessing, scores $Sc_{i,n}$ are the respective weighting factors that allow the description of the deviation of experimental spectra from their average spectrum $\boldsymbol{Sp}_{\text{av}}$ according to

$$\boldsymbol{Sp}_i = \boldsymbol{Sp}_{\text{av}} + \sum_n Sc_{i,n}\boldsymbol{L}_n \quad (4)$$

Loadings often lend themselves to a spectroscopic interpretation. Scores can provide information as to trends found within the series of experimental spectra.

Such a principal component analysis was conducted for the spectral range between 2400 cm^{-1} and 1600 cm^{-1} (very comparable results, with lower accuracy, were obtained by analyzing the entire spectral range). This region was chosen because it includes three prominent peaks that contain information on the three species of interest: D-N, D-A, and cross-links. The peak at 2268 cm^{-1} corresponds to unreacted isocyanate groups of D-N and its disappearance can be used as a measure of the degree of cross-linking.[45] The peak at 1730 cm^{-1} is attributed to the carbonyl groups of D-A, the urethane linkages, and possibly some remaining solvent.[46] Lastly, the peak at 1680 cm^{-1} is attributed to the carbonyl groups of urethane linkages and the isocyanurate rings of D-N.[46] Two loadings were considered for the PCA of the mean-centered spectra (cf. insets in Figure 3). With two loadings the variance in the data is captured by more than 99%. That is, with the given set of loadings it is possible to accurately fit the experimental data to a very high accuracy. Loading 1 is positive for the peaks corresponding to the isocyanate group (2268 cm^{-1}) and the carbonyl of the urethane linkages and isocyanurate rings (1680 cm^{-1}), while the peak at 1730 cm^{-1} is negative. Therefore, negative scores 1 correspond to a reduction of the peak intensities at 2268 and 1680 cm^{-1} and an increase of the peak intensity at 1730 cm^{-1} with respect to the average spectrum $\boldsymbol{Sp}_{\text{av}}$. Low scores correspond to a sample, with low concentrations of D-N and high concentrations of D-A. Those scores 1 are displayed in Figure 4. Note that the first principal component alone captures the variance of the data by over 96%. The increase in score 1 with increasing distance from

dx.doi.org/10.1021/co200210c | ACS Comb. Sci. 2012, 14, 415–424

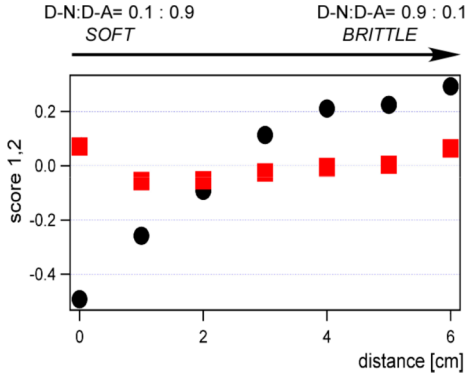

Figure 4. Scores resulting from a PCA analysis of the spectral range between 2400 and 1600 cm^{-1} of the IR data shown in Figure 3: black filled circles, score 1 (96.2% variance); and red filled squares, score 2 (3.0% variance).

the origin of the library film clearly reflects the composition of the sample. While the composition changes in a linear manner between 0 and 4 cm, this is not the case for the other positions. Only a slight variation in the chemical composition is found between 4 and 6 cm. This overall trend with regard to the sample composition is also observed in the NMR and MRI data discussed below.

Accurate description of the experimental data by using only the first principal component is only possible if, throughout the entire sample, the ratio of reacted to unreacted D-N varies linearly with the sample composition. This linearity is not necessarily expected since conversion to the polyurethane also depends on the concentration of D-A. Deviations are described by the second components, which only capture a variance of 3%. Loading 2 is also depicted in Figure 3. Loading 2 consists mostly of a positive peak at 2268 cm^{-1} (unreacted NCO) and a negative peak at 1680 cm^{-1} (urethane and isocyanurate C═O). Hence, a negative score for component 2 indicates a reduction of isocyanates with respect to an overall higher peak at 1680 cm^{-1}; that is, there is an increased formation of urethane groups. The scores 2 are also depicted in Figure 4. Note that the lowest values (i.e., highest relative conversions) are found for positions between 1 and 3 cm. The highest concentrations of urethane groups are expected where reacting functional groups are at equimolar concentrations. For an exactly linear composition variation this is expected in the middle of the film at position 3 cm. The fact that the minimum for score 2 is shifted to lower positions agrees with the overall finding of a nonlinear composition gradient.

Unfortunately, because of the lack of molar extinction coefficients and exactly known conversions it is not possible to extract quantitative information on the extent of the cross-linking. However, qualitative insight is offered from the height of the peak at 2268 cm^{-1}, the unreacted NCO group. Complete conversion of all isocyanate groups would be indicated by the complete disappearance of this peak for compositions with a stoichiometric or greater quantity of hydroxyl groups (i.e., D-N:D-A = 0.1:0.9 to D-N:D-A = 0.5:0.5). With the exception of the spectrum at 0 cm (D-N:D-A = 0.1:0.9), some signal intensity is present at 2268 cm^{-1}. Hence, conversion was not carried to completion within the majority of the gradient-composition film. As intended, a "soft" film suitable for MRI investigation was prepared by partial curing.

NMR Imaging. It was the purpose of this experimental approach to use an MRI methodology that is readily available on commercial NMR microimaging scanners. Even though the filling factor was far from optimal for our coil (20-mm diameter × 30-mm length cylinder), a reasonable signal-to-noise ratio could be achieved with a spin-echo sequence when not utilizing slice selection on a film that was 1-mm thick and 12.5-mm wide. The measured images are projections of the total signal through the sample thickness.

The shortest experimentally achievable spin-echo time (TE) was 2.1 ms. At room temperature, the signal from the polymer film decayed almost entirely during this TE (cf. eq 2), and detection of images was not possible. Heating the sample to 40 °C induced sufficient molecular mobility within the sample to lengthen the T_2 values and allow measurement of MR images using the spin-echo method, at least for the portion of the film containing the lower polyisocyanate (D-N) content. For the portion of the film containing the higher D-N content, it was even necessary to heat the sample to 60 °C. As explained in the Materials and Methods section, the 60-mm-long gradient-composition film was imaged in two separate positions since our imaging coil was 30-mm long. Analysis of the data resulted in two sets of images which are shown in Figure 5: spin-density

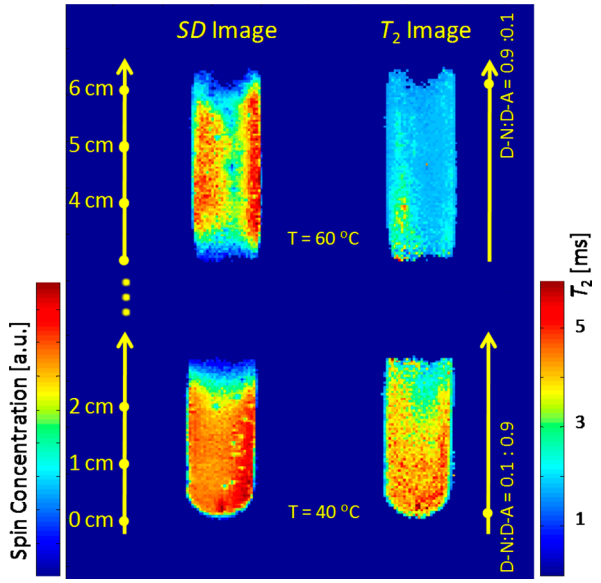

Figure 5. Parameter-selective magnetic resonance images for a gradient-composition polyurethane film prepared from a 1,6-hexamethylene diisocyanate-based polyisocyanate (D-N) and a hydroxy-terminated polyacrylate (D-A) (cf. Figure 1 for structures). The D-N:D-A ratio changes continuously from 0.1:0.9 to 0.9:0.1 over a 6-cm length of the film. The film was longer than the rf coil so the film was imaged in two sections: bottom images, marked from 0 to 3 cm, lower D-N content, 40 °C; and top images, marked from 3 to 6 cm, higher D-N content, 60 °C. On the left are spin density (SD) images that reflect a combination of ^1H concentration, sample thickness and inhomogeneities in rf excitation. On the right are T_2 images that reflect the spatial distribution of the T_2 relaxation constant, an indication of molecular mobility.

images representing the variable $SD(\mathbf{x})$, and $T_2(\mathbf{x})$ images representing the spatially resolved T_2. Spin-density images correspond mostly to the concentration of spins with respect to the sampling plane. Greater thickness at the film edges is clearly visible in the SD image taken at 60 °C. Bubbles, which lead to areas with low concentrations, are visible in the SD image taken at 40 °C. Note that the SD images may also reflect intensity

dx.doi.org/10.1021/co200210c | ACS Comb. Sci. 2012, 14, 415–424

fluctuations due to inhomogeneities in the rf-excitation profile. These fluctuations are not visible in the T_2 images since these reflect the spatial distribution of a physicochemical constant obtained through data fitting. The T_2 image of the film section taken at 40 °C shows a clear decrease of T_2 values along the long axis of the sample: T_2 decreases with increasing D-N content, which is also observable to a much lesser extent in the T_2 image taken at 60 °C. Even after raising the temperature by 20 °C, only low T_2 values are observed for the film section containing higher D-N contents.

The T_2 values can be related to other physicochemical or mechanical properties. Schneider and Simon have provided a model for the T_2 relaxation in elastomers in which several components contribute to the overall relaxation.[32,33,47] Relaxation during approximately the first millisecond is dominated by polymer chains confined by cross-links. The shape of this initial portion of the relaxation curve has been used to correlate series of elastomers with respect to their cross-link density and mechanical strength. Relaxation at longer echo times (>1 ms) is governed by free polymer chains or largely unconfined dangling chain ends. Obviously, the current NMR microimaging experiment, where the shortest achievable *TE* value is 2.1 ms, can only detect the latter moieties. As a result, the T_2 maps displayed in Figure 5 do not necessarily correlate with cross-link densities and therefore mechanical properties of the different compositions represented.

The complete recording of NMR microimaging data on elastomers and analysis to extract the cross-link density has been described.[38] However, the associated NMR method requires very short rf pulses during magnetic field gradients such that only the characterization of very small samples (a few mm) is technically feasible. Possibly, a better approach would be to combine the SPRITE or single point imaging (SPI) technique with a spin echo as demonstrated by Balcom et al.[48] We tried these techniques and encountered sensitivity issues for our films. Furthermore, argument (ii) presented in section 2 remains a concern; MRI is best suited to yield the coarse shape of characteristic relaxation functions. An approach to measure spatially resolved relaxation functions with greater accuracy is 1D NMR profiling, for which results are described below. MRI remains a very valuable method for the assessment of overall sample homogeneity and accuracy of sample preparation.

1D NMR Profiling. The feasibility of 1D NMR profiling was demonstrated by measuring simple Bloch decays. In solid samples, where the dipolar coupling between nuclei dominates over chemical shifts, it is reasonable to assume that the excitation frequencies of all ^{1}H nuclei are centered symmetrically around a characteristic frequency ω_0. Therefore, operating the spectrometer with the condition $\omega = \omega_0$ leads to a monotonically decreasing signal for $\mathrm{Re}(S(t))$ (eq 1). However, eq 1 will only hold for simple systems. Multiphase systems often exhibit nonexponential decays. Bloch decays are shown in Figure 6 for two positions along our gradient library film; nonexponential relaxation is observed and was found at all positions of the film. Close inspection of the relaxation data for $t < 50$ μs reveals a distinct deviation from exponential behavior. During the initial microseconds the slope of the decay increases with increasing time. This is a well-known finding for ^{1}H atoms experiencing strong dipolar coupling.[23] Molecules containing these ^{1}H atoms are part of a rigid framework in which no large angle motions faster than 1 kHz occur. Several functions have been discussed for the characterization of these types of decays.[23−27] For the purpose of our analysis it suffices to

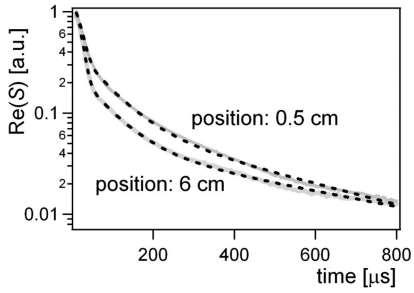

Figure 6. Bloch decays measured using the 1D NMR profiler for two positions, 0.5 and 6 cm, along the gradient-composition film: experimental data (solid line), and fit to eq 3 (dashed line). The 6-cm position contains the higher D-N content.

approximate this initial part of the decay with a Gaussian function (cf. eq 3). Further inspection of the decay curves for times >50 μs revealed continued deviation from simple exponential behavior. By using two exponential functions for this part of the decay, the entire decay curve could be fit using eq 3.

Assigning a physical meaning to all of the parameters in eq 3 can be ambiguous. It is reasonable to assume a network of cross-linked polymers that contain regions with different mobilities.[32,33,47] The most rigid moieties, with relative fraction w_{rigid}, are attributed to the highly cross-linked regions. The components of intermediate mobility ($T_{2,\mathrm{inter}}$ and w_{inter}) are attributed to lightly cross-linked chains, and the mobile component corresponds largely to free polymer chains or dangling chain ends. The presence of moisture or some remaining solvent can also contribute to the mobile component.

Altogether, the Bloch decays for all positions within the composition-gradient sample could be fitted with good accuracy using the three components represented in eq 3. Despite the quality of these fits that suggest three dynamically discrete components in the material, it is likely that a continuous transition between relaxation times and corresponding mobilities exists in these samples. Nevertheless, fitting yielded component fractions and respective T_2 values for each position along the gradient axis. No true systematic variations were found along the gradient axis for the T_2 values, which are reported here as averages over the entire film: $T_2{}^*_{,\mathrm{rigid}} = 26.3 \pm 0.8$ μs, $T_2{}^*_{,\mathrm{inter}} = 78.4 \pm 2.1$ μs, $T_2{}^*_{,\mathrm{mobile}} = 474 \pm 43$ μs. The relatively high error for $T_2{}^*_{,\mathrm{mobile}}$ may be due to improper selection of the excitation frequency ω or variations in the homogeneity of the external magnetic field, both of which are increasingly relevant with longer $T_2{}^*$ decay times.

Contrary to the $T_2{}^*$ values, the component fractions w_{mobile}, w_{inter}, and w_{rigid} vary systematically along the gradient axis (cf. Figure 7). At the low D-N content end of the film (position marked 0 cm), the film consists of about 57% rigid component, 36% intermediate, and 7% mobile component. The rigid-component fraction increases with increasing D-N content, while the mobile and intermediate component fractions decrease. The relative ratio of w_{inter} to w_{mobile} remains approximately constant throughout the sample; that is, large changes in the relative amount of free chains (mobile regions) versus lightly cross-linked chains (regions of intermediate mobility) were not observed across the sample. Hence, to a first approximation, the primary change in the dynamics of the sample can be summarized as an increase in the rigid fraction with increasing D-N (polyisocyanate) content.

dx.doi.org/10.1021/co200210c | *ACS Comb. Sci.* 2012, 14, 415−424

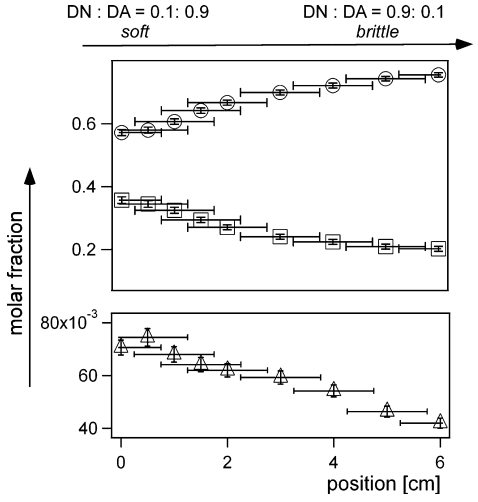

Figure 7. Molar fractions of rigid (○), intermediate (□) and mobile (△) components as determined by fitting Bloch decays obtained at different positions along a gradient-composition film (DN:DA) to eq 3. Horizontal error bars represent the spatial resolution governed by the active range of the rf coil.

The findings from 1D NMR profiling (T_2 values remain largely constant, rigid-component fraction increases with increasing D-N content) appear to contradict the findings obtained by MRI (T_2 decreases with increasing D-N content). To further investigate the apparent discrepancy between MRI and 1D NMR profiler data, spin-echo experiments were conducted at room temperature using the 1D NMR profiler. A typical spin-echo decay is displayed in Figure 8. Comparison

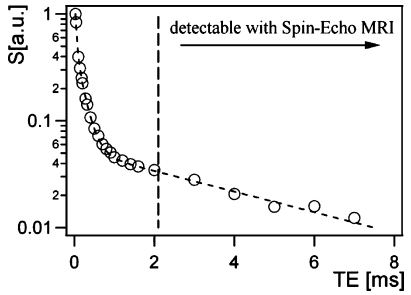

Figure 8. Spin-echo relaxation data for the position at 6 cm (high D-N content) of a gradient-composition film recorded with the 1D NMR profiler. Data for TE > 2 ms are the only ones detectable using standard MRI as described above.

with the Bloch decays depicted in Figure 6 shows some major differences:

(a) It is not possible to measure data for echo times shorter than about 30 μs. Consequently, the initial Gaussian-shaped portion of the Bloch decay, which was attributed to rigid components, is not readily apparent in the spin-echo decay. Only its final tail, which accounts for the steep decay at $TE \leq 100$ μs, is visible.

(b) For the Bloch decay the signal intensity is ~1% after 1 ms. For the spin-echo decay, around 5% of the signal intensity remains at an echo time of 1 ms. This is largely because relaxation data are normalized with respect to the first measurable data point. Since some fraction of the rigid material is undetected in the spin-echo experiment, mobile components seem to be present at higher concentrations.

(c) The spin-echo decay is measurable for echo times ranging up to 8 ms. This is because chemical shift interactions and magnetic field inhomogeneities are refocused and therefore do not contribute to signal decay to the same extent as with Bloch decays.

Note that only the tail of the spin-echo decay at TE > 2 ms is accessible via standard MRI as presented above. This tail may be described by a single exponential decay for all relaxation data. Respective time constants $T_{2,\mathrm{mobile}}$ were determined by fitting spin-echo data for TE > 2 ms using eq 2. Good fits could be obtained for all positions along the gradient in the library film. The $T_{2,\mathrm{mobile}}$ relaxation times, displayed in Figure 9, decrease with increasing D-N content. This indicates the film becomes more rigid with increasing D-N content, which is consistent with the MRI data shown in Figure 5.

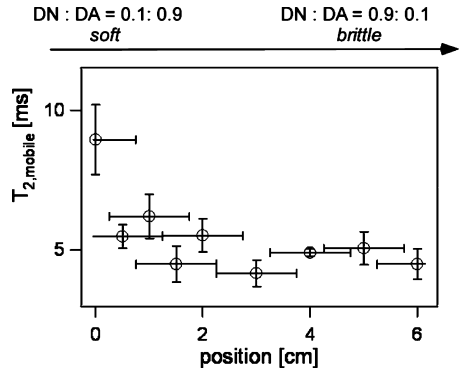

Figure 9. Mobile-component spin−spin relaxation times, $T_{2,\mathrm{mobile}}$, obtained by fitting the spin-echo data collected for TE > 2 ms at different positions along the gradient in a library film using the 1D NMR profiler. Horizontal error bars represent the spatial resolution determined by the active range of the rf coil. The position marked 0 cm contains the lowest D-N (i.e., polyisocyanate) content.

Overall, NMR data from Bloch and spin-echo decays appear very consistent with the mechanical properties of the film. Close to the position marked 0 cm (D-N:D-A = 0.1:0.9) the film is soft and flexible, while it is brittle close to the position marked 6 cm (D-N:D-A = 0.9:0.1). The increase in D-N content primarily causes an increase in the rigid-component fraction. Decreases in the mobility of the mobile fraction are minor, and only detectable using the spin-echo sequence. The increased amount of the rigid fraction likely contributes toward the increased mechanical brittleness in this material. However, the rigid domains may also act as cross-linking and reinforcing agents that further increase the rigidity of the mobile domains to increase the hardness of the film.

5. CONCLUSIONS

Polymer films with gradient compositions may be used as convenient libraries for the assessment of mechanical properties of polymeric materials. Nuclear magnetic resonance is a powerful tool to investigate underlying molecular and physicochemical properties in these gradient films through a variety of NMR-determined parameters. NMR imaging (i.e., MRI) provides a means to assess the spatial distribution of these NMR parameters. However, the hard- and software limitations associated with MRI characterization of polymer films, which can exhibit a large variety of properties, will likely

dx.doi.org/10.1021/co200210c | ACS Comb. Sci. 2012, 14, 415−424

require development of experimental protocols on a case by case basis. It should be kept in mind that the tremendous progress in clinical MRI is essentially based on optimizing the technique for one single sample: the human body. Standard MRI for the characterization of polymer-based gradient-composition films appears to be suitable for evaluation of overall film quality provided sufficient molecular mobility is present. This limitation is much less of an issue for existing NMR spectroscopic methods. A modern NMR spectrometer with solid-state NMR capabilities (high power for rf pulses and fast analog-to-digital converter) is capable of characterizing materials with underlying molecular mobilities ranging from those encountered in rigid crystalline or amorphous phases to liquid melts. A whole array of methods exist to characterize these materials with respect to cross-link density, molecular mobility, and phase composition.[19,20,27] The 1D profiling method demonstrated in this paper provides a convenient means to use static NMR methods on gradient-composition samples. Moreover, since signal sensitivity is much less of an issue for the 1D NMR profiler than it is for MRI, it is practical to study nuclei other than ^{1}H, including ^{19}F, ^{13}C, ^{2}H, ^{15}N, and ^{31}P in thin solid films.

AUTHOR INFORMATION

Corresponding Author

*E-mail: johannes.leisen@chemistry.gatech.edu.

Funding

Funding from the Dow Chemical Company is gratefully acknowledged.

Notes

The authors declare no competing financial interest.

REFERENCES

(1) Zweifel, H., Ed.; *Plastics Additives Handbook*, 5th ed.; Carl Hanser Verlag: Munich, Germany, 2001.

(2) Webster, D. C. Combinatorial and high-throughput methods in macromolecular materials research and development. *Macromol. Chem. Phys.* **2008**, *209*, 237−246.

(3) Genzer, J.; Bhat, R. R. Surface-bound soft matter gradients. *Langmuir* **2008**, *24*, 2294−2317.

(4) Webster, D. C.; Chisholm, B. J.; Stafslien, S. J. Mini-review: Combinatorial approaches for the design of novel coating systems. *Biofouling* **2007**, *23*, 179−192.

(5) Maier, W. F.; Stowe, K.; Sieg, S. Combinatorial and high-throughput materials science. *Angew. Chem., Int. Ed.* **2007**, *46*, 6016−6067.

(6) Kohn, J.; Welsh, W. J.; Knight, D. A new approach to the rationale discovery of polymeric biomaterials. *Biomaterials* **2007**, *28*, 4171−4177.

(7) Amis, E. J. Reaching beyond discovery. *Nat. Mater.* **2004**, *3*, 83−85.

(8) Meredith, J. C. Advances in Combinatorial and High-Throughput Screening of Biofunctional Polymers for Gene Delivery, Tissue Engineering and Anti-Fouling Coatings. *J. Mater. Chem.* **2009**, *19*, 34−45.

(9) Meredith, J. C.; Karim, A.; Amis, E. J. Combinatorial Methods for Investigations in Polymer Materials Science. *MRS Bull.* **2002**, *27*, 330−335.

(10) Gomez, I.; Basak, P.; Meredith, J. C. Polymer Thickness and Composition Gradients. In *Soft Matter Gradient Surfaces: Methods and Applications*; Genzer, J., Ed.; Wiley: New York, 2012.

(11) Zapata, P.; Su, J.; Garcia, A.; Meredith, J. C. Quantitative High-Throughput Screening of Osteoblast Attachment, Spreading, and Proliferation on Demixed Polymer Blend Micropatterns. *Biomacromolecules* **2007**, *8*, 1907−1917.

(12) Simon, C. G.; Stephens, J. S.; Dorsey, S. M.; Becker, M. L. Fabrication of combinatorial polymer scaffold libraries. *Rev. Sci. Instrum.* **2007**, *78*, 072207.

(13) Julthongpiput, D.; Fasolka, M. J.; Zhan, W. H.; Nguyen, T.; Amis, E. J. Gradient chemical micropatterns: A reference substrate for surface nanometrology. *Nano Lett.* **2005**, *5*, 1535−1540.

(14) Sung, H. J.; Su, J.; Berglund, J. D.; Russ, B. V.; Meredith, J. C.; Galis, Z. S. The use of temperature−composition combinatorial libraries to study the effects of biodegradable polymer blend surfaces on vascular cells. *Biomaterials* **2005**, *26*, 4557−4567.

(15) Gent, A. N. *Engineering with rubber*; Carl Hanser Verlag: Munich, Germany, 2001.

(16) Yao, N.; He, W.; Liu, G.; Lam, K. S. Applications of nuclear magnetic resonance spectroscopy (NMR) to combinatorial chemistry. *Huaxue Jinzhan* **2004**, *16*, 696−707.

(17) Shapiro, M. J. Combinatorial chemistry: NMR applications. In *Encyclopedia of Nuclear Magnetic Resonance*; Wiley: New York, 2002; Vol. *9*, pp 514−519.

(18) Keifer, P. A. Flow NMR applications in combinatorial chemistry. *Curr. Opin. Chem. Biol.* **2003**, *7*, 388−394.

(19) Duer, M. J. *Solid-state NMR spectroscopy, principles and applications*; Blackwell Science: Oxford, U.K., 2002.

(20) Schmidt-Rohr, K.; Spiess, H. W. *Multidimensional solid-state NMR and polymers*; Academic Press: London, U.K., 1994.

(21) Gilman, J. W.; Bourbigot, S.; Shields, J. R. High throughput methods for polymer nanocomposites research: Extrusion, NMR characterization and flammability property screening. *J. Mater. Sci.* **2003**, *38*, 4451−4460.

(22) Bourbigot, S.; Vanderhart, D. L.; Gilman, J. W. Investigation of nanodispersion in polystyrene-montmorillonite nanocomposites by solid-state NMR. *J. Polym. Sci., Part B: Polym. Phys.* **2003**, *41*, 3188−3213.

(23) Hansen, E. W.; Kristiansen, P. E.; Pedersen, B. Crystallinity of Polyethylene Derived from Solid-State Proton NMR Free Induction Decay. *J. Phys. Chem. B* **1998**, *102*, 5444−5450.

(24) Kristiansen, P. E.; Hansen, E. W.; Pedersen, B. Phase distribution in polyethylene versus temperature probed by solid-state proton NMR free induction decay. *Polymer* **1999**, *41*, 311−321.

(25) Kristiansen, P. E.; Hansen, E. W.; Pedersen, B. Phase Distribution during Isothermal Crystallization of Polyethylene Probed by Solid-State Proton NMR Free Induction Decay. *J. Phys. Chem. B* **1999**, *103*, 3552−3558.

(26) Kristiansen, P. E.; Hansen, E. W.; Pedersen, B. Isothermal crystallization of polyethylene monitored by in situ NMR and analyzed within the "Avrami" model framework. *Polymer* **2000**, *42*, 1969−1980.

(27) Yamanobe, T.; Uehara, H.; Kakiage, M. Practical NMR Analysis of Morphology and Structure of Polymers. *Annu. Rep. NMR Spectrosc.* **2010**, *70*, 203−239.

(28) Sotta, P.; Fuelber, C.; Demco, D. E.; Bluemich, B.; Spiess, H. W. Effect of Residual Dipolar Interactions on the NMR Relaxation in Cross-Linked Elastomers. *Macromolecules* **1996**, *29*, 6222−6230.

(29) Fechete, R.; Demco, D. E.; Blumich, B. Enhanced sensitivity to residual dipolar couplings of elastomers by higher-order multiple-quantum NMR. *J. Magn. Reson.* **2004**, *169*, 19−26.

(30) Demco, D. E.; Hafner, S.; Fuelber, C.; Graf, R.; Spiess, H. W. Two-dimensional proton magnetization-exchange NMR spectroscopy in cross-linked elastomers. *J. Chem. Phys.* **1996**, *105*, 11285−11296.

(31) Graf, R.; Demco, D. E.; Hafner, S.; Spiess, H. W. Selective residual dipolar couplings in crosslinked elastomers by ^{1}H double-quantum NMR spectroscopy. *Solid State Nucl. Magn. Reson.* **1998**, *12*, 139−152.

(32) Simon, G.; Schneider, H. Mc determination in elastomers by proton-NMR relaxation and deuterium NMR spectroscopy. *Makromolekulare Chemie, Macromolecular Symposia* **1991**, *52*, (Eur. Symp. Polym. Spectrosc., 9th, 1990), 233−246.

(33) Simon, G.; Schneider, H.; Haeusler, K. G. Proton NMR transversal relaxation in crosslinked 1,4-cis-polybutadiene. *Prog. Colloid Polym. Sci.* **1988**, *78*, (Relat. Polym. Struct. Prop.), 30−32.

(34) Hayashi, S.; Komori, Y. Determination of residual dipolar interaction from transverse ^{1}H NMR relaxation in elastomers. *Solid State Nucl. Magn. Reson.* **2009**, *36*, 167−171.
(35) Bluemich, B. *NMR Imaging of Materials*; Clarendon Press: Oxford, U.K., 2000.
(36) Codd, S. L.; Seymour, J. D., Eds.; *Magnetic Resonance Microscopy*; Wiley-VCH: Weinheim,Germany, 2009.
(37) Hoegemann, D.; Ntziachristos, V.; Josephson, L.; Weissleder, R. High Throughput Magnetic Resonance Imaging for Evaluating Targeted Nanoparticle Probes. *Bioconjugate Chem.* **2002**, *13*, 116−121.
(38) Kuhn, W.; Barth, P.; Hafner, S.; Simon, G.; Schneider, H. Material Properties Imaging of Cross-Linked Polymers by NMR. *Macromolecules* **1994**, *27*, 5773−5779.
(39) Schneider, M.; Demco, D. E.; Blumich, B. ^{1}H NMR Imaging of Residual Dipolar Couplings in Cross-Linked Elastomers: Dipolar-Encoded Longitudinal Magnetization, Double-Quantum, and Triple-Quantum Filters. *J. Magn. Reson.* **1999**, *140*, 432−441.
(40) Zhang, Z.; Martin, J.; Wu, J.; Wang, H.; Promislow, K.; Balcom Bruce, J. Magnetic resonance imaging of water content across the Nafion membrane in an operational PEM fuel cell. *J. Magn. Reson.* **2008**, *193*, 259−266.
(41) Holly, R.; Keller, B. M.; Pignol, J.-P.; Lemaire, C.; Peemoeller, H. Initial investigation on the use of MR spectroscopy and micro-MRI of GAFCHROMIC EBT radiotherapy film. *Med. Phys.* **2009**, *36*, 5341−5346.
(42) Beyea, S. D.; Balcom, B. J.; Prado, P. J.; Cross, A. R.; Kennedy, C. B.; Armstrong, R. L.; Bremner, T. W. Relaxation time mapping of short T2* nuclei with single-point imaging (SPI) methods. *J. Magn. Reson.* **1998**, *135*, 156−164.
(43) Bluemich, B.; Casanova, F. Mobile NMR. *Mod. Mag. Reson.* **2006**, *1*, 369−378.
(44) Kubista, M.; Nygren, J.; Elbergali, A.; Sjoeback, R. Making Reference Samples Redundant. *Crit. Rev. Anal. Chem.* **1999**, *29*, 1−28.
(45) Wang, F. C.; Feve, M.; Lam, T. M.; Pascault, J.-P. FTIR Analysis of Hydrogen Bonding in Amorphous Linear Aromatic Polyurethanes. I. Influence of Temperature. *J. Polym. Sci., Part B: Polym. Phys.* **1994**, *32*, 1305−1313.
(46) Radice, S.; Turri, S.; Scicchitano, M. Fourier Transform Infrared Studies on Deblocking and Crosslinking Mechanisms of Some Fluorine Containing Monocomponent Polyurethanes. *Appl. Spectrosc.* **2003**, *58*, 535−542.
(47) Simon, G.; Goetschmann, B.; Matzen, D.; Schneider, H. Proton NMR spin-spin relaxation in crosslinked SBR with and without carbon black filling. *Polym. Bull.* **1989**, *21*, 475−482.
(48) Petrov, O.; Ersland, G.; Balcom, B. J. T_2 Distribution Mapping Profiles with Phase Encode MRI. *J. Magn. Reson.* **2011**, *209*, 39−46.